scientific reports

Check for updates

OPEN

Biosynthesis of silver nanoparticles via *Melaleuca alternifolia* leaf extract for antibacterial, antifungal, antioxidant and anticancer activity

B. Mary Dayana[1,9], Raja Venkatesan[3,4]✉, J. Thomas Joseph Prakash[2]✉, P. Saravanan[5], M. Sherlin Nivetha[6], Adhigan Murali[3,9], Alexandre A. Vetcher[7], Munusamy Settu[8] & Seong-Cheol Kim[3]✉

Synthesis of silver nanoparticles using the leaf extract of *Melaleuca alternifolia* (M-AgNPs), as evidenced by various physicochemical characterizations, including UV-Visible spectroscopy (UV-Vis), Fourier-transform infrared spectroscopy (FT-IR), dynamic light scattering (DLS), X-ray diffraction (XRD), scanning electron microscopy (SEM), energy-dispersive X-ray analysis (EDAX), high-resolution transmission electron microscopy (HR-TEM), and zeta potential analysis. The UV-Vis spectrum exhibited a characteristic absorption peak at 402 nm, confirming the formation of M-AgNPs. FT-IR analysis identified the presence of various functional groups associated with the silver nanoparticles. DLS measurements indicated a hydrodynamic size of 45.79 nm with a polydispersity index (PDI) of 0.335. Zeta potential analysis revealed a value of -21 mV, suggesting good stability of the nanoparticles. XRD analysis showed a crystalline size of 25.47 nm and confirmed the face-centered cubic (FCC) structure. SEM images revealed well-defined and uniformly dispersed nanoparticles. EDAX confirmed the presence of silver at the elemental level. HR-TEM analysis demonstrated that the actual size of the nanoparticles was approximately 10 nm. Antimicrobial studies demonstrated the effectiveness of the synthesized nanoparticles against both bacterial and fungal strains. The antioxidant activity of the M-AgNPs was measured at 41.17 µL/mL. Furthermore, cytotoxicity studies showed that the nanoparticles exhibited an IC_{50} value of 8.16 µg/mL against MCF-7 breast cancer cells. The synthesized M-AgNPs possess significant potential as therapeutic agents, particularly against MCF-7 cancer cells, and may serve as promising candidates for future medical applications.

Keywords *Melaleuca alternifolia* extract, Silver nanoparticles, Zeta potential, antibacterial, Antifungal, Antioxidant, Anticancer activity

Nanotechnology enables the production of materials at the atomic or molecular scale, typically with dimensions of less than 100 nm[1]. At the nanoscale, materials exhibit unique properties such as a large surface-to-volume ratio and quantum effects. The increased surface area per unit mass allows a larger number of atoms to interact with their surroundings[2]. Silver has been described as "dynamic" due to its excellent potential for biological

[1]Department of Physics, St. Joseph's College, (Affiliated to Bharathidasan University, Tiruchirappalli 620002, Tamil Nadu, India. [2]PG & Research Department of Physics, Government Arts College (Affiliated to Bharathidasan University), Tiruchirappalli 620022, Tamil Nadu, India. [3]School of Chemical Engineering, Yeungnam University, 280 Daehak–Ro, Gyeongsan 38541, Republic of Korea. [4]Department of Biomaterials, Saveetha Dental College and Hospitals, SIMATS, Saveetha University, Chennai 600077, Tamil Nadu, India. [5]Department of Chemistry, St. Joseph's College of Engineering, OMR, Chennai 600119, Tamil Nadu, India. [6]Department of Chemistry, Sathyabama Institute of Science and Technology (Deemed to be University), Vadamangalam, Sriperumbudur 602108, Tamil Nadu, India. [7]Institute of Pharmacy and Biotechnology (IPhB), RUDN University n.a. P. Lumumba (RUDN), 6 Miklukho-Maklaya Str, Moscow 117198, Russian Federation. [8]Centre for Applied Nanomaterials, Chennai Institute of Technology, Chennai 600069, Tamil Nadu, India. [9]B. Mary Dayana and Adhigan Murali contributed equally to this work. ✉email: rajavenki101@gmail.com; armyjpr1@yahoo.co.in; sckim07@ynu.ac.kr

applications, including antifungal, antibacterial, antiviral, anti-infectious, wound healing, and anti-inflammatory properties, even at low concentrations[3–5]. These small particles are known as nanoparticles, which can be produced using either top-down or bottom-up approaches. To achieve specific applications, it is often necessary to modify certain properties and parameters such as pH, temperature, and molar concentration during nanoparticle synthesis. Silver nanoparticles (AgNPs) have a complex three-layer structure[6]. The outermost layer facilitates functionalization with other molecules such as metal ions or polymers. The core and outer layers are connected by an intermediate layer, which is chemically distinct from the core. The substance of the nanoparticle resides in the core layer, and the most crucial aspect of its three-layer structure is the synthesis or processing technique used. Nanoparticle production methods are broadly classified into two categories: top-down and bottom-up. Top-down approaches involve reducing the size of larger particles to the nanoscale[7–10]. In contrast, bottom-up approaches, which are considered more efficient, involve creating nanoparticles from smaller molecules and controlling their size through chemical concentration and reaction conditions[11].

Green chemistry is a design framework that aims to create molecules, materials, and processes that are non-hazardous to both human health and the environment. It represents a preventive approach that is applied at the earliest stages of developing new chemical entities and technologies[12]. The organic synthesis of nanoparticles using plant extracts is referred to as green nanotechnology or green synthesis, and the resulting nanoparticles are known as biogenic nanoparticles. Silver nanoparticles have been synthesized from a wide range of medicinal plants[13]. Cancer is characterized by uncontrolled cell division and the subsequent invasion of healthy cells and tissues. According to the American Cancer Society, there will be an estimated 21.7 million new cases of cancer worldwide by 2030. A study published by the IMS Health Institute for Healthcare Informatics in 2015 reported that the global market for cancer therapies reached a record high of US$107 billion, with projections to reach US$150 billion by 2020. Based on rising cancer rates, the incidence is expected to increase by 60% by 2030. Severe side effects often accompany cancer treatments[14]. Due to their size, shape, and unique optical and thermal properties, nanoparticles are being used in both the diagnosis and treatment of cancer. Recent research highlights the significant role of biological methods in the synthesis of metal nanoparticles[15–18].

Our aim is to synthesize silver nanoparticles (AgNPs) using the aqueous extract of *Melaleuca alternifolia* through an eco-friendly green synthesis approach, and to evaluate their physicochemical characteristics and multifunctional bioactivities. These include assessing their antibacterial, antifungal, antioxidant, and anticancer properties, thereby exploring their potential for therapeutic and biomedical applications. Earlier studies have shown that the antimicrobial activity of *Melaleuca alternifolia* is largely driven by its major bioactive compounds.

Experimental section

Collection of plant materials

Young and healthy leaves of *Melaleuca alternifolia* were collected from the Ooty, Tamil Nadu, India. *Melaleuca alternifolia*, the plant material used in this study, was officially recognized by taxonomists at the Department of Botany, St. Joseph's College, Tiruchirappalli 620,002, India. A voucher specimen bearing accession number (8170), which is accessible to the public, has been added to the Departmental Herbarium. This enables it to be replicated and utilized as a future reference. The freshly harvested leaves were thoroughly rinsed with distilled water to eliminate any adhered dust or surface contaminants. After washing, the leaves were spread out evenly and dried under shade for a period of two weeks to ensure complete removal of moisture, which is essential for effective extraction and long-term storage. *Melaleuca alternifolia* plant material was collected in accordance with institutional and local regulations. No special permits or licenses were required for this activity because *Melaleuca alternifolia* is not a protected or endangered species and the gathering was held in areas that were open to the public.

Preparation of *Melaleuca alternifolia* extract

The plant was shade-dried at room temperature and then pulverized into a coarse powder using a sterile mortar and pestle. A measured quantity of 2 g of this powdered plant material was added to 100 mL of distilled water. The mixture was allowed to stand at room temperature for 10 min to allow initial extraction of phytochemicals. Following this, the solution was gently heated using a heating mantle at 60 °C for 10 min to enhance the extraction efficiency of bioactive compounds. After heating, the mixture was allowed to cool to room temperature and subsequently filtered through Whatman No.1 filter paper to remove any solid residues. The resulting clear aqueous extract was collected and stored in a sterile container at 4 °C for further use in nanoparticle synthesis.

Synthesis of silver nanoparticles

To synthesize silver nanoparticles, 20 mL of the previously prepared *Melaleuca alternifolia* leaf extract was mixed with 80 mL of a 1 mM aqueous solution of silver nitrate ($AgNO_3$) under sterile conditions. The *Melaleuca alternifolia* leaf extract was mixed with 1 mM $AgNO_3$solution under continuous stirring, and nanoparticle formation was monitored by the characteristic color change and UV–Vis absorption peak[19]. The reaction mixture was kept at room temperature and observed for any visible color change, which indicates the reduction of Ag^+ ions to silver nanoparticles (Ag^0). The formation of a brownish color in the solution served as a preliminary confirmation of nanoparticle synthesis, owing to the surface plasmon resonance phenomenon exhibited by silver nanoparticles, M-AgNPs.

Characterization

The synthesized M-AgNPs were characterized using UV-Vis spectroscopy and their reduction mediated by plant extracts. The biologically reduced, brown-colored solution was precisely scanned using a PerkinElmer

Lambda 365 spectrophotometer. The chemical composition of the synthesized M-AgNPs was analyzed using a PerkinElmer FTIR spectrometer in the range of 400–4000 cm^{-1}. Zeta potential measurements were carried out using a Zetasizer Nano ZS to determine the surface charge of the nanoparticles. Dynamic light scattering (DLS) was used to determine the hydrodynamic size and polydispersity index (PDI) of the nanoparticles, using a Micromeritics NanoPlus analyzer. X-ray diffraction (XRD) analysis was performed using a PANalytical $X'Pert^3$ instrument. The surface morphology and elemental composition of the synthesized M-AgNPs were examined using scanning electron microscopy (SEM) combined with energy-dispersive X-ray spectroscopy (EDAX), carried out on a Tescan Vega3 Inca system (Oxford Instruments). The shape, size, and particle distribution of the green-synthesized M-AgNPs were observed using high-resolution transmission electron microscopy (HR-TEM) with a JEOL JEM-2100 electron microscope.

Biological studies

Antibacterial activity

The antibacterial activity of silver nanoparticles was investigated against strains of clinical pathogenic microorganisms using the disc diffusion method. All the bacterial strains were purchased from the Microbial Type Culture and Collection (MTCC) at Chandigarh, India. The media used for the antifungal test was Sabouraud's dextrose agar/broth of Hi Media, Bombay, India.

Antioxidant assay

The 2,2-diphenyl-1-picrylhydrazyl (DPPH) free radical scavenging experiment to test how well the M-AgNPs we made worked as antioxidants. In our study, the DPPH working solution was prepared at a concentration of 1 µL/mL DPPH, dissolved in methanol. This concentration was used consistently throughout the antioxidant assay to evaluate the free radical scavenging activity of the M-AgNPs. We mixed different amounts of M-AgNPs with a methanolic DPPH solution and let them sit in the dark at room temperature for 30 min. A UV-Vis spectrophotometer was used to quantify the drop in absorbance at 517 nm. We employed ascorbic acid as a positive control.

Anticancer activity

The human cancer cell lines were cultured in DEME as a monolayer with heat-inactivated 10% FBS and 1% antibiotic. The shape of cancer cells after the treatment of synthesized M-AgNPs was studied under an inverted microscope.

Cell culture maintenance

Dulbecco's Modified Eagle's Medium, streptomycin, penicillin-G, L-glutamine, phosphate buffered saline, 3-(4,5 dimethylthiozol-2-yl)-2,5-diphenyltetrazoliumbromide, 2'7'diacetyl dichloro fluorescein, sodium didecyl sulphate, trypan blue, trypsin-EDTA, ethylene diamine tetra acetic acid, triton X-100, ethanol, dimethyl sulfoxide (DMSO), and bovine serum albumin were purchased from Sigma Aldrich Chemicals Pvt. Ltd (India). All other chemicals used were of analytical grade, purchased from Hi media Laboratories Pvt. Ltd., India. Cell lines for Breast cancer were obtained from the Cell repository of National Centre for Cell Sciences (NCCS), Pune, India. The cell line was maintained in Dulbecco's Modified Eagle Medium (DMEM), supplemented with 10% Fetal Bovine Serum (FBS). To avoid bacterial contamination, 100 µg/mL of streptomycin and 100 U/mL of Penicillin were added to the medium. Cell line media was kept at 37 °C in a humidified atmosphere with 5% CO_2.

Results and discussion

UV-Visible spectroscopy

The synthesis of silver nanoparticles was confirmed with UV Vis spectroscopic analysis, and the result was depicted in Fig. 1A. In essence, the brown colour associated with the surface plasmon resonance (SPR) is a unique visual characteristic of metal nanoparticles[20]. The presence of free electrons in the synthesized M-AgNPs are responsible for the formation of the SPR absorption band. SPR is created when these unbound electrons reciprocally vibrate with the light waves[21]. The maximum absorbance peak was observed at 402 nm, confirming that the Melaleuca alternifolia aqueous extract reduced Ag^+ to Ag^0, thereby synthesizing nanoparticles. Figure 1A displays a broad bell-shaped spectrum curve of UV-Vis spectroscopy of the synthesized M-AgNPs. Various metabolites from the plant extract introduced into the solution broaden the plasmon band[22,23]. Figure 1B,C shows the direct and indirect band gap of synthesized M-AgNPs.

FTIR spectroscopy

The FTIR spectrum of the synthesized M-AgNPs is shown in (Fig. 2A). The functional groups are responsible for the bio reduction of Ag^+ to the Ag^0 state of the phytochemicals. The obtained spectrum shows the presence of various chemical constituents. The N-H stretching mode in protein linking was attributed to the strong broad band at 3429 cm^{-1}. The existence of proteins as capping agent for the M-AgNPs is shown by the peak at 1641 cm^{-1} which corresponds to the C = O stretching mode in the amine I group, which is frequently present in proteins[24]. The UV-Vis spectra are linked to the C-C and C-N vibrations of the chlorophyll tetrapyrrole ring, which are primarily responsible for the peak at 1041 cm^{-1} and 1383 cm^{-1}. The findings imply that the plant leaf extract's free functional groups may bind metal nanoparticles while encasing or capping them to stop them from clumping together. Proteins and other biological substances serve two purposes: (a) reduction of Ag^+ ions to Ag^0 and (b) Silver nanoparticles stabilization in the aqueous medium. Bands at 2919 cm^{-1} and 2842 cm^{-1} region arising from C-H stretching of aromatic compound were observed[25]. Terpinen-4-ol, which is already well recognized for its strong antimicrobial and anti-inflammatory properties. When these phytochemicals interact

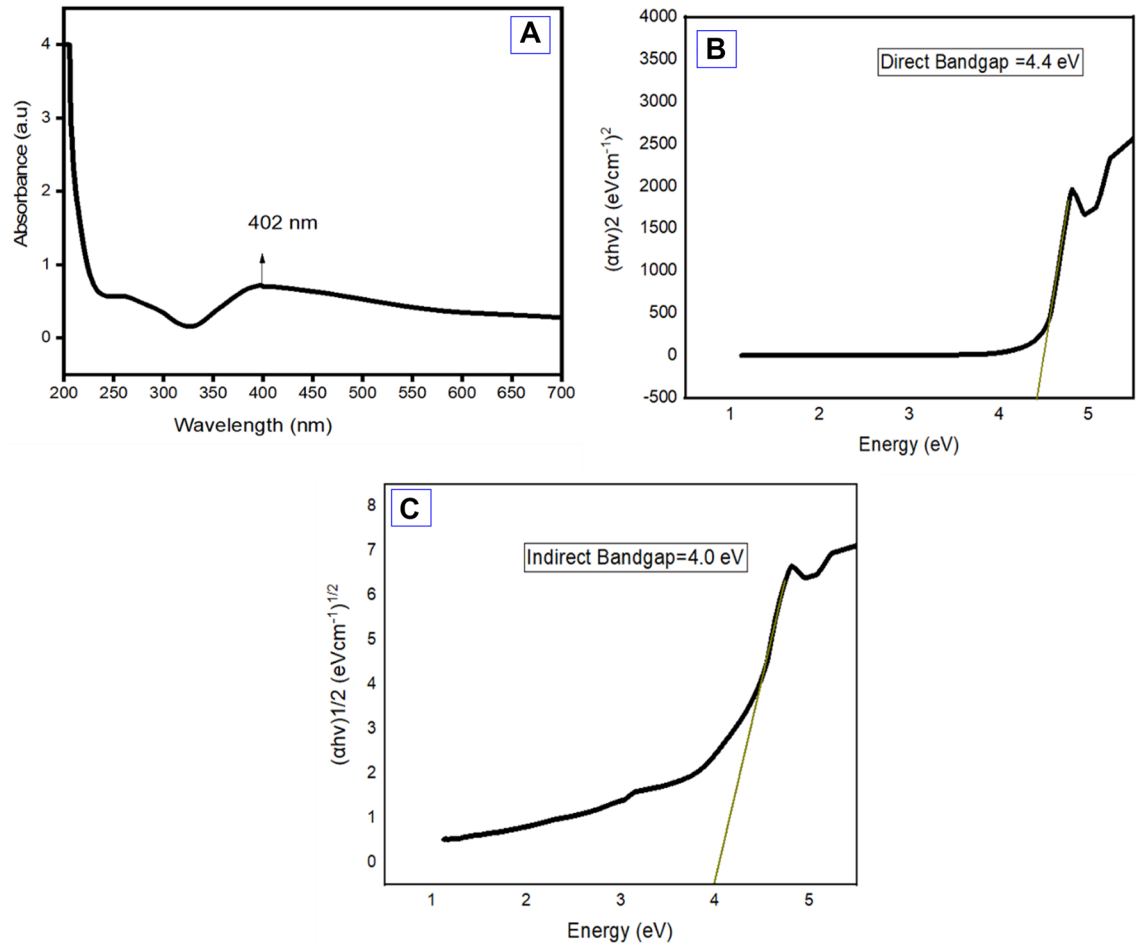

Fig. 1. (**A**) UV Vis spectroscopy of synthesized M-AgNPs, (**B**) Direct band gap of M-AgNPs, and (**C**) Indirect band gap of synthesized M-AgNPs.

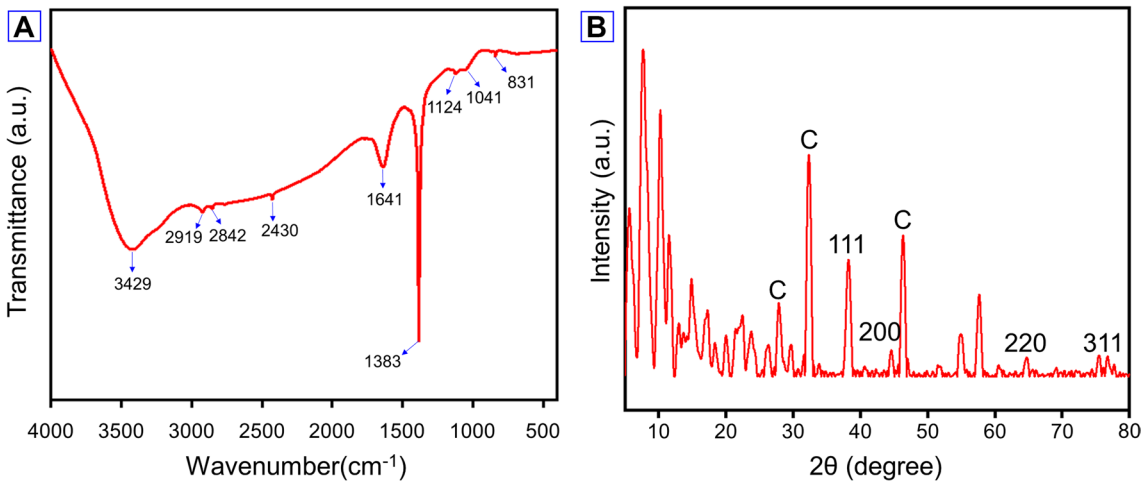

Fig. 2. (**A**) FITR, and (**B**) XRD patterns of synthesized M-AgNPs.

with biosynthesized AgNPs, the combination can generate synergistic effects, often resulting in enhanced activity against skin- and oral-associated pathogens, including drug-resistant strains[26].

XRD analysis

The X -ray diffraction pattern of synthesized M-AgNPs is shown in (Fig. 2B). A number of strong reflections were observed at 2θ of 38°, 44°, 64°, 77°. The face centered cubic lattice structure of the biosynthesized M-AgNPs is confirmed by these diffraction peaks which correlate to the (111), (200), (220), (311) planes of M-AgNPs (JCPDS file no. 03-065-2871). The unit cell(a) edge or lattice parameter for the material with fcc crystal structure is 4.07 Å (JCPDS file no.04-0783). We calculated the lattice constant using the equation $a = d\,x\sqrt{(h^2 + k^2 + l^2)}$. It was 4.07Å. our results exactly matches with JCPDS value[27]. Peaks at 2θ = 27.7°, 32.1°, 46.3° in (Fig. 2B), are matches to carbon (JCPDS file no. 18–0311) which is likely to originate from the organic encapsulation of M-AgNPs[28].

Dynamic light scattering (DLS) and zeta potential

The hydrodynamic diameter, its effective size as it moves through a fluid, considering its shape, interaction with the fluid and any surrounding layers which can be measured by DLS technique. This technique is used in many scientific and industrial applications due to non-invasiveness, quick measurement and capacity to analyse a wide range of particle sizes. It is based on the ideas of examining variation of intensity of scattered light brought on by the Brownian motion of the particles[25]. When nanoparticles are disseminated in liquids, a tiny layer of the solvent's electric dipole is adsorbed at their surface.

The hydrodynamic diameter describes the metal core with any stabiliser material and the solvent layer since this layer influences the mobility of the particles in the solution. Consequently, DLS determines the size of the nanoparticles by attaching solvent molecules with their surface. In colloidal solutions, the diameter of the nanoparticles rises when one layer of the stabilizer is adsorbed at their surface; frequently there are several layers of stabilisers and water molecules are present. Thus, in DLS measurements, the protective layer and the interaction with the solvent molecules are considered[27]. The particle size distribution of the synthesized M-AgNPs (Fig. 3A). It was found that the M-AgNPs hydrodynamic diameter is 45.79 nm with PDI value of 0.335. This indicates the mono dispersity of synthesized M-AgNPs. The larger DLS diameter (45.79 nm) compared to the TEM core diameter (~ 10 nm) likely reflects an organic capping/binder layer (from extract phytochemicals) plus solvation and any small dynamic aggregates; DLS measures hydrodynamic diameter and is intensity-weighted, whereas TEM measures the dry metallic core[28].

Nanoparticles with zeta potential value greater than + 30 mV or less than − 30 mV were shown to be stable because of their strongly cationic and strongly anionic nature. Highly stable nanoparticles that avoid the agglomeration condition[29,30]. Figure 3B shows the zeta potential value of synthesized M-AgNPs. It shows the zeta potential value of -21mV. Effective interaction with positively charged bacteria and fungus are made possible by the negative charge on the surface. As a result, their biocompatibility is enhanced[31].

SEM analysis with EDAX

SEM and EDAX techniques were used to analyse the sample in order to obtain a better understanding of the characteristics of the synthesized M-AgNPs. Figure 4A,B shows SEM image and EDAX of synthesized M-AgNPs. Using EDAX on the SEM, the element analysis of the silver nanoparticles was carried out[32,33]. The peak at about 3.2 KeV represent the binding energy of the Ag. SEM provided further insight into the morphology and size details of the synthesized M-AgNPs. SEM was used to characterize the morphology, size and size distribution of synthesized M-AgNPs. The SEM image synthesized M-AgNPs at 200 nm level, particles are well defined cubical in shape (Fig. 4A). It is an FCC structure which exhibit poly crystalline nature. Particles are not agglomerated. The EDX of the M-AgNPs was performed to investigate the elemental composition of the biosynthesized M-AgNPs. The EDX reveals a strong signal at 3.2 KeV, which is generally shown by metallic silver nanocrystals due to surface plasmon resonance. The other metal ions like carbon, oxygen also appeared in the EDX spectrum. Figure 4B shows the EDAX image of synthesized M-AgNPs[34].

HR-TEM analysis

Figure 5A displays the biosynthesized M-AgNPs and a high-resolution transmission electron microscopy (HR-TEM) image. The nanoparticles in the HR-TEM micrograph (Fig. 5A) are primarily spherical, evenly dispersed, and exhibit no agglomeration, suggesting a stable colloidal dispersion. The strong crystallinity and poly dispersed character of the produced nanoparticles are confirmed by the distinct contrast and well-defined edges[22]. According to the HR-TEM image's particle size analysis, the average size is roughly 10 nm, as seen in Fig. 5B. Since smaller nanoparticles often exhibit improved surface reactivity and cellular uptake, this nanoscale dimension aligns well with the desired properties for biomedical and antibacterial applications. The matching SAED pattern, consisting of a series of concentric rings with bright spots, is shown in Fig. 5C. These rings demonstrate the polycrystalline nature of the AgNPs. According to the XRD results, the different diffraction rings match the (111), (200), (220), and (311) planes of face-centered cubic (FCC) silver[35]. The clarity and sharpness of the diffraction spots further support the crystalline structure and great purity of the produced silver nanoparticles.

Biological studies

Antibacterial activity of M-AgNPs

The disc diffusion method, the antibacterial activity of M-AgNPs was ascertained. Using Muller Hinton Agar, the petri dishes (diameter 60 mm) were made and inoculated with test organisms. 10 µL of Amoxicillin, silver, plant extract, and nanoparticles were each deposited onto a sterile disc that was 6 mm wide. For compound

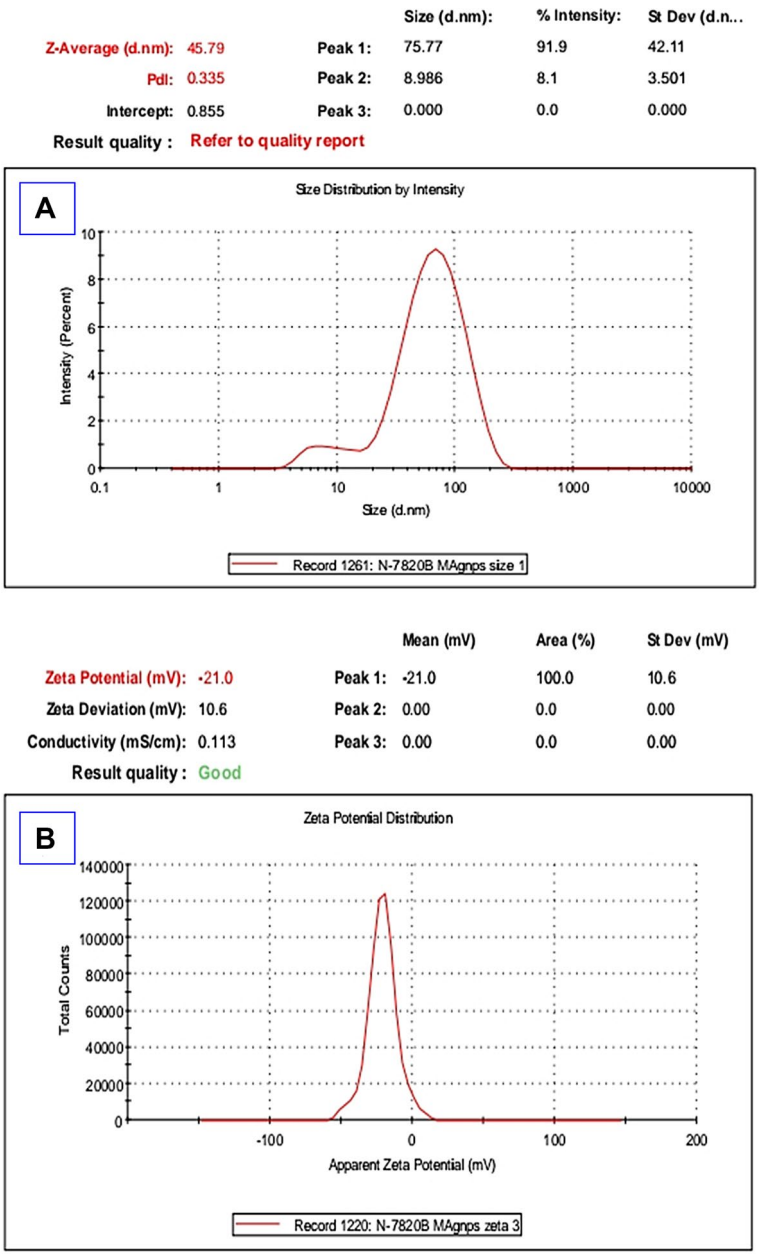

Fig. 3. (**A**) DLS studies, and (**B**) Zeta potential of synthesized M-AgNPs.

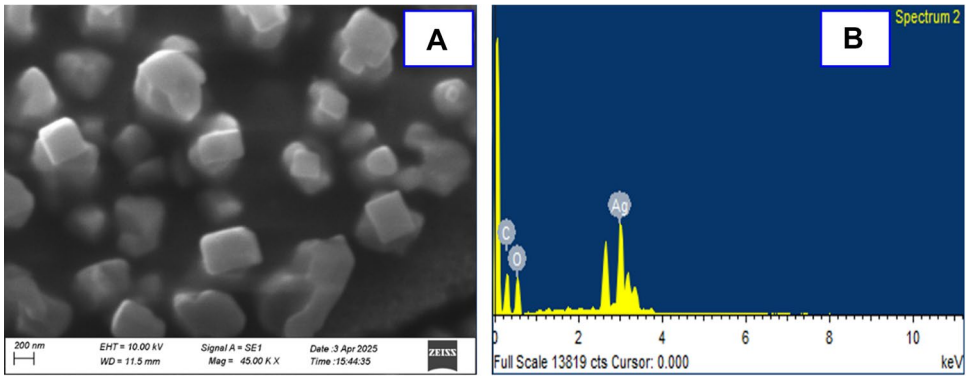

Fig. 4. (**A**) SEM image of synthesized M-AgNPs, and (**B**) EDAX of M-AgNPs.

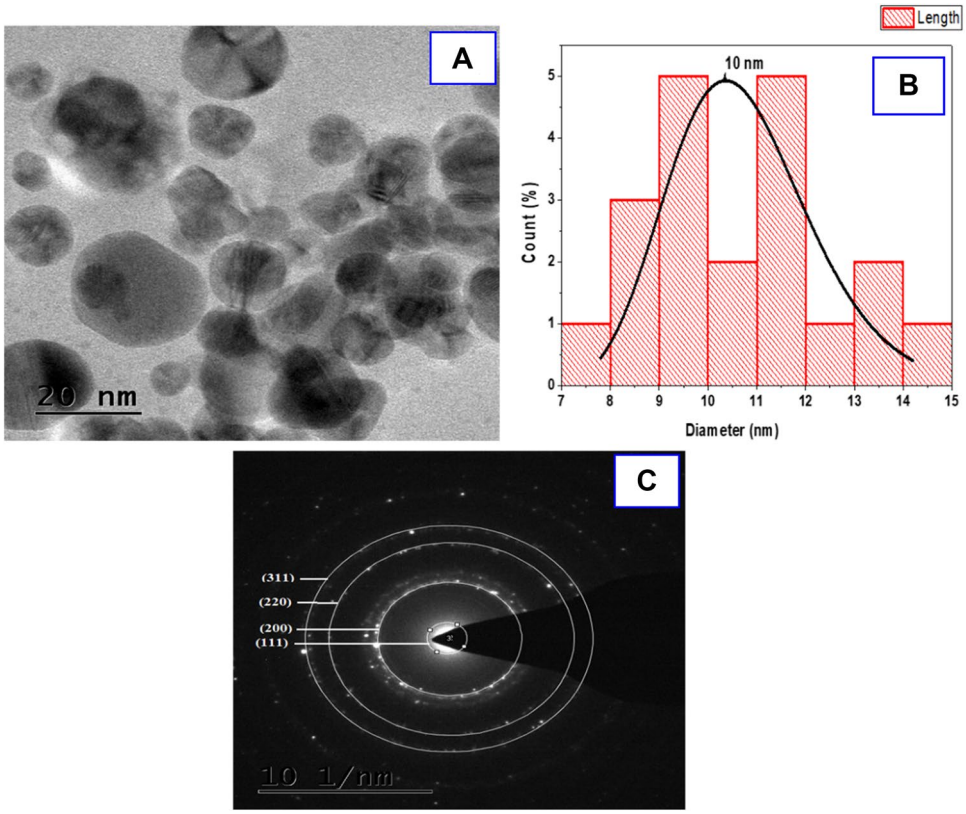

Fig. 5. (**A**) HR-TEM image, (**B**) Histogram, and (**C**) SAED pattern of synthesized M-AgNPs.

diffusion, prepared discs were positioned on top of the agar plates and allowed to sit at room temperature for 30 min. As a conventional antibiotic disc, 10 µL of Amoxicillin was used to provide the positive control and a solution of 1 mM $AgNO_3$ was used as the blank control[36]. The experiment was conducted thrice, and the zone of inhibition was measured in millimeters after the plates were incubated for 24 h at 37 °C. The antibacterial potential of synthesized M -AgNps was tested against the gram-positive bacterial strains *Staphylococcus epidermis* (Fig. 6A), *Bacillus cereus* (Fig. 6B) and gram-negative bacterial strains *Pseudomonas aeruginosa* (Fig. 6C), *Streptococcus pyogenes* (Fig. 6D). Synthesized nanoparticles show great potential for gram-negative bacterial strains, *Pseudomonas aeruginosa* (MTCC 1688), and *Streptococcus pyogenes* (MTCC 442) than for gram-positive bacterial strains. Synthesized M-AgNPs nanoparticles showed the zone of inhibition of 7.3 ± 0.9 mm for *Pseudomonas aeruginosa* and 7.0 ± 1.2 mm for *Streptococcus pyogenes*.

Table 1 showed the zone of inhibition of M-AgNPs for different bacterial strains. Results showed that synthesized M-AgNPs are more susceptible to *Pseudomonas aeruginosa* and *Streptococcus pyogenes*. At the concentration of 10 µL/mL, M-AgNPs show the zone of inhibition of 7.3 ± 0.9 mm and 7.0 ± 1.2 mm Increasing the surface area of nanoparticles has been found to enhance their effectiveness, as it also increases their surface energy[37–40]. Consequently, even at low concentrations, smaller nanoparticles with a higher surface area to volume ratio show strong antibacterial properties. Additionally, it was noted in a report that gram-negative bacteria showed a maximum zone of inhibition. This could be because gram-positive bacteria's cell walls are made up of a thick layer of peptidoglycan, which forms a rigid structure and makes it difficult for M-AgNPs to penetrate, whereas gram-negative bacteria's cell walls are made up of a thinner layer of peptidoglycan[41]. Cell cations released from M-AgNPs, which serve as a reservoir of Ag^+ ions are unquestionably responsible for the significant bacterial activity. It is hypothesized that these ions from the NPs will adhere to the negatively charged bacterial cell walls and cause them to burst, denaturing proteins and leading to cell death[42–45].

Determination of antifungal activity

Antifungal activity of sample M-AgNPs was determined using the disc diffusion method The petridishes (diameter 60 mm) was prepared with Sabouraud's dextrose agar (SDA) and inoculated with test organisms. Sterile disc of 6 mm width was impregnated with 10 µL of Fluconazole, silver, plant extract and nanoparticles[46]. Prepared discs were placed onto the top layer of the agar plates and left for 30 min at room temperature for compound diffusion. As a conventional antibiotic disc 10 µl of Fluconazole was used to create a positive control and a solution of 1 mM $AgNO_3$ was used as the blank control. The zone of inhibition was measured in millimeters after the dishes were incubated for 24 h at 37 °C. *Aspergillus fumigatus* (Fig. 7A) was shown to be more responsive to the synthesized M-AgNPs than *Candida tropicalis* (Fig. 7B). Table 2 shows the zone of inhibition of M-AgNPs for different fungal strains. For *Aspergillus fumigatus*, the zone of inhibition was 6 mm, while for *Candida tropicalis*, it was 4 mm[47,48]. Synthesized M-AgNPs are more potential against *Aspergillus*

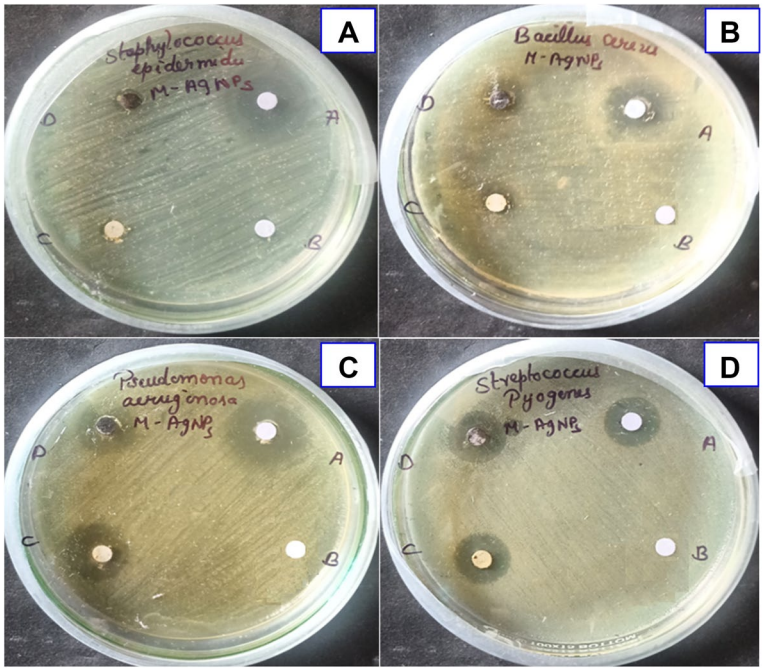

Fig. 6. Antibacterial activity of the synthesized L-AgNPs, (**A**) *Staphylococcus epidermis*, (**B**) *Bacillus cereus*, (**C**) *Pseudomonas aeruginosa*, and (**D**) *Streptococcus pyogenes*.

Samples	Concentrations (µL/mL)	Zone of Inhibition (in mm) (Diameter)			
		Staphylococcus epidermidis	Bacillus cereus	Pseudomonas aeruginosa	Streptococcus pyogenes
A (Amoxicillin)	10	11.1 ± 0.5	8.3 ± 1.9	10.0 ± 0.6	8.9 ± 0.8
B (1mM $AgNO_3$)	10	-	-	-	-
C (Plant extract)	10	-	2.0 ± 1.0	6.1 ± 0.4	5.1 ± 0.1
D (Nanoparticles)	10	1.0 ± 0.5	3.1 ± 1.7	7.3 ± 0.9	7.0 ± 1.2

Table 1. Antibacterial activity of M-AgNPs.

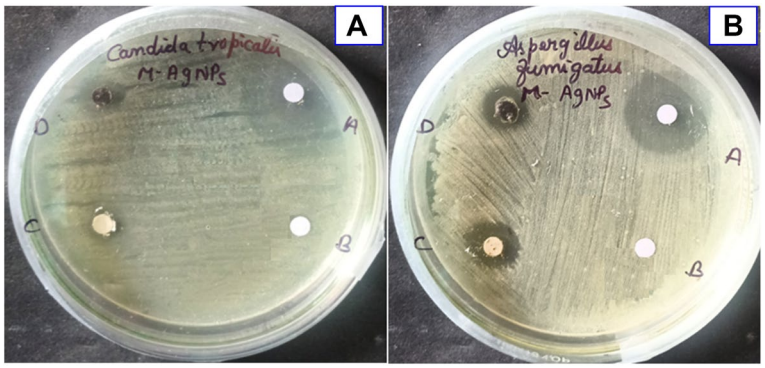

Fig. 7. Antifungal activity of synthesized L-AgNPs, (A) *Candida tropicalis*, and (B) *Aspergillus fumigatus*.

fumigatus than *Candida tropicalis*. At the concentration of 10 µL/mL, M-AgNPs were found to display high antifungal activity towards *Aspergillus fumigatus* and it shows the zone of inhibition of 6 mm[49,50]. Disruption of cell membrane formation and further stoppage of fungal reproduction in *Aspergillus fumigatus* is due to the action of M-AgNPs. Silver nanoparticles synthesized using *Melaleuca alternifolia* (tea tree) extracts show many features common to plant-mediated AgNPs, but some important differences arise from the tea-tree's chemistry (high terpene/terpinen-4-ol content) versus polyphenol-rich extracts from other medicinal plants. Several

S. No	Samples	Concentrations (µL/mL)	Zone of Inhibition (in mm) (Diameter)	
			Candida tropicalis	Aspergillus fumigatus
1.	A (Fluconazole)	10	12	11
2.	B (1mM $AgNO_3$)	10	-	-
3.	C (Plant extract)	10	1	5
4.	D (Nanoparticles)	10	4	6

Table 2. Antifungal activity of L-AgNPs.

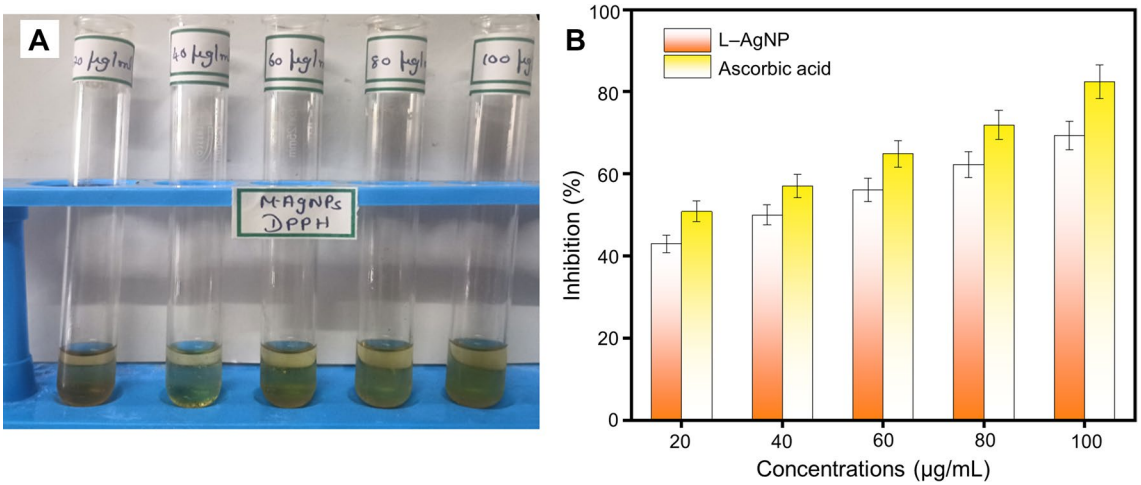

Fig. 8. (**A**) Antioxidant of the synthesized M-AgNPs, (**B**) Compared to ascorbic acid by the DPPH assay method.

S. No	Concentrations (µL/mL)	Antioxidant activity DPPH (%)	
		M-AgNPs	Ascorbic acid
1.	20	42.98	50.87
2.	40	50.0	57.01
3.	60	56.14	64.91
4.	80	62.28	71.92
5.	100	69.29	82.45
6.	IC_{50}	41.17	20.48

Table 3. Antioxidant activity of L-AgNPs by DPPH assay method.

recent studies report that tea-tree–mediated nanoparticles exhibit good antimicrobial activity against skin/oral pathogens and can act synergistic effect with antimicrobials[51].

Antioxidant activity

The antioxidant activity of the synthesized M-AgNPs is illustrated in Fig. 8, compared to conventional ascorbic acid. The results demonstrate that the samples exhibit a substantial concentration of antioxidant activity[52]. The results show that the samples exhibit good antioxidant activity at high concentrations. The aqueous extract exhibits 69.29% antioxidant activity at a concentration of 100 µL/mL, whereas ascorbic acid shows 82.45% at the same concentration[53–55]. The proton radical scavenging action is attributed to antioxidants, as measured by the DPPH radical scavenging assay. Table 3 shows the antioxidant activity of the sample at elevated concentration, and its activity is compared with ascorbic acid, and 1000 µL of distilled water served as the blank. DPPH radical scavenging at five concentrations (20, 40, 60, 80, 100 µL/mL) was measured. M-AgNPs showed concentration-dependent scavenging (42.98%, 50.00%, 56.14%, 62.28%, 69.29% at 20–100 µL/mL, respectively). The IC_{50} (concentration producing 50% scavenging) was calculated from linear regression of the dose–response curve and found to be 41.17 µL/mL for M-AgNPs, compared with 20.48 µL/mL for ascorbic acid (positive control). All measurements were performed in triplicate and data are presented. Our synthesized nanoparticles showed an IC_{50} value of 41.17 µL/mL while ascorbic acid showed 20.48 µL/mL of antioxidant property.

Anticancer activity

The mitochondrial dehydrogenase of living cells reduces the yellow 3–4,5 dimethylthiozol-2-Yl)-2,5diphenyltetrazoliumbromide (MTT) producing a detectable purple formation product. NAD (P) H-dependent reductase, which is present in viable cells, converts the MTT reagent to formazan, a deep purple substance. After dissolving the Formazan crystals with a solubilising solution, the absorbance is measure by a plate reader 500–600 nm. MTT (50 mg) dye was dissolved in 10 mL of PBS. After vortexing for 1 min, it was filtered through 0.45 micro filters. The bottle was wrapped with aluminium foil to prevent light, as MTT was light sensitive. The preparation was stored at 4 °C.

Following their collection and haemocytometer count, the MCF-7 viable cells were diluted in DMEM medium to a density of 1×10^4 cells/ml planted in 96 well plates per well and incubated for 24 h to facilitate adhesion. MCF-7 cells were incubated for 24 h at 37 °C in a humidified 95% air and 5% CO_2 incubator with varying doses of C-P (5 to 25 µg/mL). Following incubation, the drug containing cells were rinsed with new culture media and each well was filled with MTT (5 mg/mL in PBS) solution before being cultured for an additional 4 h at 37 °C. Using a microplate reader, the absorbance at 540 nm was used to determine the cell viability after the purple precipitated formazan was dissolved in 100 µL of DMSO. The percentage of live cells compared to the control was used to express the results. The viability percentage was calculated using the following formula:

$$\text{Cell viability}(\%) = \frac{\text{Mean absorbence of the control} - \text{Mean absorbence of the control}}{\text{Mean absorbence of the control}}$$

The IC_{50} values were determined from the C-P dose responsive curve where inhibition of 50% cytotoxicity compared to control cells. All experiments were performed at least three times in triplicate. Figure 9A–F shows cell death of MCF – 7 Breast cancer cells for the different concentrations of synthesized M-AgNPs. The further in vitro study focused to MCF-7 cell line, which is resistant to many kinds of anticancer drugs and to evaluate the sensitivity of this cell lines[56–58].

The microscopic images reveal progressive morphological alterations in MCF-7 cells—including shrinkage, detachment, membrane blebbing, and loss of structural integrity—following treatment with M-AgNPs at concentrations of 2.5, 5.0, 7.5, 10.0, and 15.0 µg/mL for 24 h, compared with the untreated control. The control cells retained normal, intact morphology, as observed under an inverted microscope. Consistent with these morphological changes, elevated concentrations of M-AgNPs led to substantial cell death. The cytotoxic response was further quantified using the MTT assay[59–62], which demonstrated a clear dose-dependent decline in cell viability. The M-AgNPs produced an IC_{50} value of 8.16 µg/mL, as depicted in Fig. 10.

Conclusion

The current study demonstrated that silver nanoparticles (M-AgNPs) can be synthesized in a green manner using *Melaleuca alternifolia* leaf extract. UV-Vis spectroscopy revealed a characteristic surface plasmon resonance peak at 402 nm, confirming the formation of nanoparticles. FTIR examination revealed functional groups, including hydroxyl, amine, and carbonyl, which suggests that they played a role in the processes of reduction

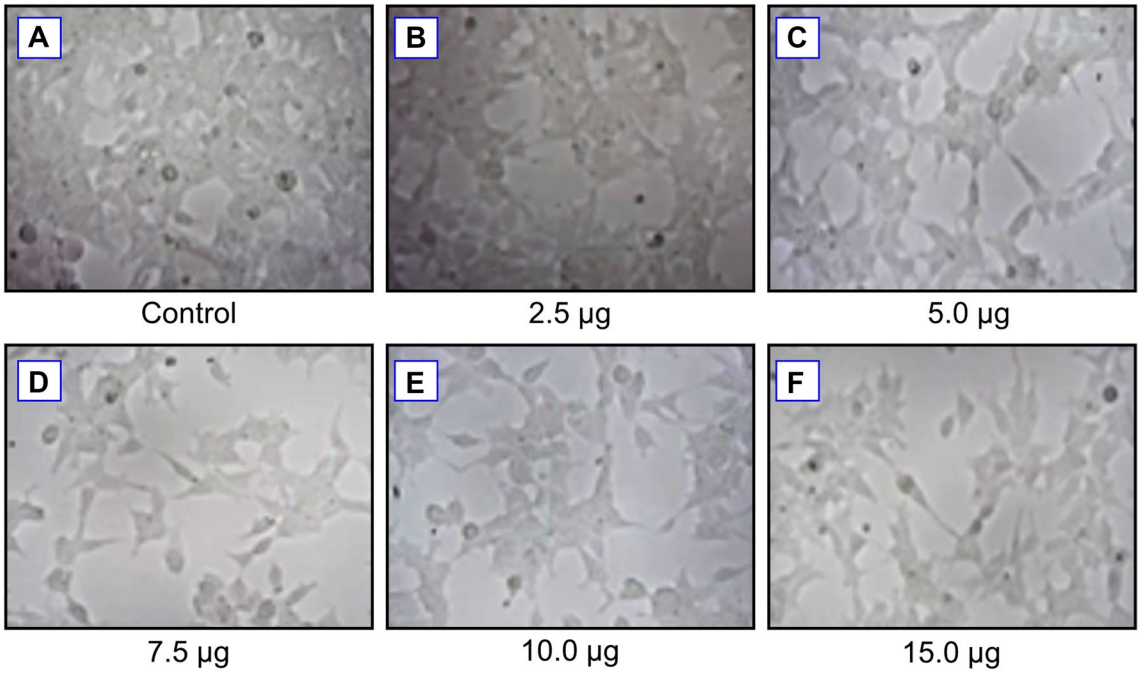

Fig. 9. Morphological changes in control and sample M-AgNPs treated MCF – 7 Breast cancer cells for 24 h, (**A**) Control, (**B**) 2.5 µg, (**C**) 5 µg, (**D**) 7.5 µg, (**E**) 10 µg, and (**F**) 15 µg.

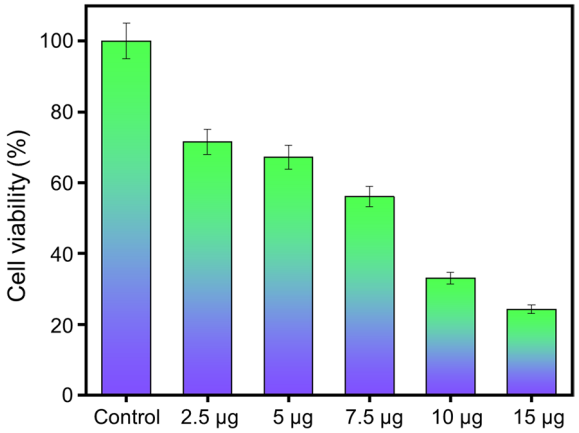

Fig. 10. Cell viability of synthesized M-AgNPs.

and stabilization. The DLS measurements showed a hydrodynamic diameter of 45.79 nm and a polydispersity index (PDI) of 0.335. The zeta potential analysis yielded a value of − 21 mV, confirming that the sample was somewhat stable. XRD investigation revealed that the crystalline structure was face-centered cubic (FCC) and that the average crystallite size was 25.47 nm. SEM and EDAX tests showed that the nanoparticles were cubical, spread out well, and contained silver. HR-TEM also demonstrated that the nanoparticles were poly dispersed and spherical, with an average size of about 10 nm. Different SAED patterns confirmed the strong crystallinity. The M-AgNPs made by living things were very effective at killing bacteria, especially *Pseudomonas aeruginosa* and *Streptococcus pyogenes*, with a maximal zone of inhibition7.3 ± 0.9 mm. Tests for antifungal activity showed that *Aspergillus fumigatus* was more sensitive to the antifungal agent than *Candida tropicalis*. The DPPH experiment demonstrated that the substance exhibited a strong scavenging effect, with an IC_{50} value of 41.17 µL/mL, comparable to that of normal ascorbic acid. In addition, the anticancer activity against MCF-7 breast cancer cells demonstrated a high dose-dependent cytotoxic effect, with an IC_{50} value of 8.16 µg/mL, and visible changes in shape indicative of apoptosis. Overall, the work demonstrates that M-AgNPs can be synthesized through biosynthesis and exhibit strong antibacterial, antioxidant, and anticancer properties demonstrate preliminary potential. Future research should focus on establishing standardized and reproducible synthesis protocols, developing scalable production strategies suitable for industrial applications.

Data availability

The datasets used and/or analysed during the current study available from the corresponding author on reasonable request.

Received: 14 August 2025; Accepted: 9 December 2025
Published online: 20 January 2026

References

1. Khan, I., Saeed, K. & Khan, I. Nanoparticles: Properties, applications and toxicities. *Arab. J. Chem.* **12**, 908–931. https://doi.org/10.1016/j.arabjc.2017.05.011 (2019).
2. Joudeh, N. & Linke, D. Nanoparticle classification, physicochemical properties, characterization, and applications: A comprehensive review for biologists. *J. Nanobiotechnol.* **20**, 262. https://doi.org/10.1186/s12951-022-01477-8 (2022).
3. Sasikumar, T., Kumar, J. V., Rhim, J. W., Shin, G. H. & Kim, J. T. Yellow–emitting carbon Dots as 'off–on' fluorescence probes in paper–based micro kit for selective detection of silver ions and Kanamycin in animal–derived food. *J. Environ. Chem. Eng.* **13**, 117706. https://doi.org/10.1016/j.jece.2025.117706 (2025).
4. Dhaka, A., Mali, S. C., Sharma, S. & Trivedi, R. A review on biological synthesis of silver nanoparticles and their potential applications. *Results Chem.* **6**, 101108. https://doi.org/10.1016/j.rechem.2023.101108 (2023).
5. Galdiero, S. et al. Silver nanoparticles as potential antiviral agents. *Molecules* **16**, 8894–8918. https://doi.org/10.3390/molecules16108894 (2011).
6. Najafloo, R., Behyari, M., Imani, R. & Nour, S. A mini-review of thymol incorporated materials: applications in antibacterial wound dressing. *J. Drug Deliv Sci. Technol.* **60**, 101904. https://doi.org/10.1016/j.jddst.2020.101904 (2020).
7. Pérez-Santonja, J. J., Güell, J. L., Gris, O., Vázquez Dorrego, X. M. & Pellicer, E. Benítez-Del-Castillo, liposomal ozonated oil in ocular infections: a review of preclinical and clinical studies, focusing on its antiseptic and regenerative properties. *Clin. Ophthalmol.* **16**, 1953–1962. https://doi.org/10.2147/OPTH.S360929 (2022).
8. Manikandan, V. et al. Metal-organic frameworks (MOFs): multifunctional platforms for environmental sustainability. *Chem. Rec.* **25**, e202400257. https://doi.org/10.1002/tcr.202400257 (2025).
9. Bandurska, K., Berdowska, A., Barczyńska-Felusiak, R. & Krupa, P. Unique features of human Cathelicidin LL-37. *BioFactors* **41**, 289–300. https://doi.org/10.1002/biof.1225 (2015).
10. Niculescu, A. G. & Grumezescu, A. M. Natural compounds for preventing ear, nose, and throat-related oral infections. *Plants* **10**, 1847. https://doi.org/10.3390/plants10091847 (2021).
11. de Macedo, L. M. et al. Rosemary (*Rosmarinus officinalis* L., syn salvia Rosmarinus Spenn.) and its topical applications: A review. *Plants* **9**, 651. https://doi.org/10.3390/plants9050651 (2020).

12. Alsahag, M. et al. Preparation of carboxymethyl cellulose/polyvinyl alcohol wound dressing composite immobilized with anthocyanin extract for colorimetric monitoring of wound healing and prevention of wound infection. *Int. J. Biol. Macromol.* **224**, 233–242. https://doi.org/10.1016/j.ijbiomac.2022.10.119 (2023).
13. Alharbi, N. S., Alsubhi, N. S. & Felimban, A. I. Green synthesis of silver nanoparticles using medicinal plants: characterization and application. *J. Radiat. Res. Appl. Sci.* **15**, 109–124. https://doi.org/10.1016/j.jrras.2022.06.012 (2022).
14. Alaysuy, O. et al. Development of green and sustainable smart biochromic and therapeutic bandage using red cabbage (Brassica Oleracea L. Var. capitata) extract encapsulated into alginate nanoparticles. *Int. J. Biol. Macromol.* **211**, 390–399. https://doi.org/10.1016/j.ijbiomac.2022.05.062 (2022).
15. Arul, V. et al. Visible-light-driven photocatalytic degradation of amoxicillin using $FeMoO_2$/chitosan/CdO nanocomposite for sustainable water treatment. *Polym. Adv. Technol.* **36**, e70097. https://doi.org/10.1002/pat.70097 (2025).
16. Ilieva, Y., Zaharieva, M. M., Najdenski, H. & Kroumov, A. D. Antimicrobial activity of *Arthrospira* (former *Spirulina*) and *Dunaliella* related to recognized antimicrobial bioactive compounds. *Int. J. Mol. Sci.* **25**, 5548. https://doi.org/10.3390/ijms25105548 (2024).
17. Ma, Y. et al. Advances of Cobalt nanomaterials as anti-infection agents, drug carriers, and immunomodulators for potential infectious disease treatment. *Pharmaceutics* **14**, 2351. https://doi.org/10.3390/pharmaceutics14112351 (2022).
18. Ali, B. et al. Essential oils used in aromatherapy: A systemic review. *Asian Pac. J. Trop. Biomed.* **5**, 601–611. https://doi.org/10.1016/j.apjtb.2015.05.007 (2015).
19. Siavash & Iravani Green synthesis of metal nanoparticles using plants. *Green. Chem.* **13**, 2638. https://doi.org/10.1039/c1gc15386b (2011).
20. Jiang, Z., Li, L., Huang, H., He, W. & Ming, W. Progress in laser ablation and biological synthesis process: top-down and bottom-up approaches for the green synthesis of Au/Ag nanoparticles. *Int. J. Mol. Sci.* **23**, 23. https://doi.org/10.3390/ijms232314658 (2022).
21. Chan, H. K. & Kwok, P. C. L. Production methods for nanodrug particles using the bottom-up approach. *Adv. Drug Deliv Rev.* **63**, 406–416. https://doi.org/10.1016/j.addr.2011.03.011 (2011).
22. Rahuman, H. B. H. et al. Medicinal plants mediated the green synthesis of silver nanoparticles and their biomedical applications. *IET Nanobiotechnol.* **16**, 115–144. https://doi.org/10.1049/nbt2.12078 (2022).
23. Baron, E. P. Medicinal properties of cannabinoids, terpenes, and flavonoids in cannabis, and benefits in migraine, headache, and pain: an update on current evidence and cannabis science. *Headache: J. Head Face Pain*. **58**, 1139–1186. https://doi.org/10.1111/head.13345 (2018).
24. Korinek, M. et al. Anti-inflammatory and antimicrobial volatile oils: fennel and Cumin inhibit neutrophilic inflammation via regulating calcium and MAPKs. *Front. Pharmacol.* **12**, 674095. https://doi.org/10.3389/fphar.2021.674095 (2021).
25. Chen, B. K. & Wang, C. K. Electrolyzed water and its Pharmacological activities: A mini-review. *Molecules* **27**, 1222. https://doi.org/10.3390/molecules27041222 (2022).
26. Carson, C. F., Hammer, K. A. & Riley, T. V. *Melaleuca alternifolia* (tea tree) oil: A review of antimicrobial and other medicinal properties. *Clin. Microbiol. Rev.* **19**, 50–62. https://doi.org/10.1128/cmr.19.1.50-62.2006 (2006).
27. Missana, T., Benedicto, A., Mayordomo, N. & Alonso, U. Analysis of anion adsorption effects on alumina nanoparticles stability. *Appl. Geochem.* **49**, 68–76. https://doi.org/10.1016/j.apgeochem.2014.04.003 (2014).
28. Velgosova, O., Dolinská, S., Podolská, H., Mačák, L. & Čižmárová, E. Impact of plant extract phytochemicals on the synthesis of silver nanoparticles. *Materials* **17**, 2252. https://doi.org/10.3390/ma17102252 (2024).
29. Ramos, J., Forcada, J. & Hidalgo-Alvarez, R. Cationic polymer nanoparticles and nanogels: from synthesis to biotechnological applications. *Chem. Rev.* **114**, 367–428. https://doi.org/10.1021/cr3002643 (2014).
30. Mdarhri, H. A. et al. Kettani-Halabi, alternatives therapeutic approaches to conventional antibiotics: advantages, limitations and potential application in medicine. *Antibiotics* **11**, 1826. https://doi.org/10.3390/antibiotics11121826 (2022).
31. Hudson, J. B. Applications of the phytomedicine *Echinacea purpurea* (Purple Coneflower) in infectious diseases. *J. Biomed. Biotechnol.* **1**, 769896. https://doi.org/10.1155/2012/769896 (2012).
32. Favela-Camacho, S. E., Samaniego-Benítez, E. J., Godinez-Garcia, A. & Avilés-Arellano, L. M. Pérez-Robles, how to decrease the agglomeration of magnetite nanoparticles and increase their stability using surface properties. *Colloids Surf. A: Physicochem Eng. Asp.* **574**, 29–35. https://doi.org/10.1016/j.colsurfa.2019.04.016 (2019).
33. Yeap, S. P., Lim, J., Ooi, B. S. & Ahmad, A. L. Agglomeration, colloidal stability, and magnetic separation of magnetic nanoparticles: collective influences on environmental engineering applications. *J. Nanopart. Res.* **19**, 368. https://doi.org/10.1007/s11051-017-4065-6 (2017).
34. Jiang, J., Oberdörster, G. & Biswas, P. Characterization of size, surface charge, and agglomeration state of nanoparticle dispersions for toxicological studies. *J. Nanopart. Res.* **11**, 77–89. https://doi.org/10.1007/s11051-008-9446-4 (2009).
35. Soenen, S. J., Parak, W. J., Rejman, J. & Manshian, B. (eds), (Intra) cellular stability of inorganic nanoparticles: Effects on cytotoxicity, particle functionality, and biomedical applications. *Chem. Rev*. 115 2109–2135. (2015). https://doi.org/10.1021/cr400714j
36. Alam, M. A. et al. Crystallinity integration and crystal growth behavior study of preferred oriented (111) cubic silver nanocrystal. *Inorg. Chem. Commun.* **173**, 113834. https://doi.org/10.1016/j.inoche.2024.113834 (2025).
37. Liu, F. et al. Green biosynthesis and characterization of organic fructus mori-composite silver nanoparticles: enhanced antioxidant and antibacterial activities. *Mater. Today Commun.* **39**, 108837. https://doi.org/10.1016/j.mtcomm.2024.108837 (2024).
38. Anastas, P. & Eghbali, N. Green chemistry: principles and practice. *Chem. Soc. Rev.* **39**, 301–312. https://doi.org/10.1039/B918763B (2010).
39. Ovais, M. et al. Green synthesis of silver nanoparticles via plant extracts: beginning a new era in cancer theranostics. *Nanomedicine* **11**, 3157–3177. https://doi.org/10.2217/nnm-2016-0279 (2016).
40. Salem, S. S. et al. Antibacterial, cytotoxicity and larvicidal activity of green synthesized selenium nanoparticles using *Penicillium corylophilum*. *J. Clust Sci.* **32**, 351–361. https://doi.org/10.1007/s10876-020-01794-8 (2020).
41. Sooraj, M. P., Nair, A. S. & Vineetha, D. Sunlight-mediated green synthesis of silver nanoparticles using *Sida retusa* extract and assessment of its antimicrobial and catalytic activities. *Chem. Pap.* **75**, 351–363. https://doi.org/10.1007/s11696-020-01304-0 (2020).
42. Veeraraghavan, V. P. et al. Green synthesis of silver nanoparticles from aqueous extract of *Scutellaria Barbata* and coating on the cotton fabric for antimicrobial applications and wound healing activity in fibroblast cells (L929). *Saudi J. Biol. Sci.* **28**, 3633–3640. https://doi.org/10.1016/j.sjbs.2021.05.007 (2021).
43. Pirtarighat, S., Ghannadnia, M. & Baghshahi, S. Green synthesis of silver nanoparticles using the plant extract of *Salvia spinosa* grown in vitro and their antibacterial activity assessment. *J. Nanostruct. Chem.* **9**, 1–9. https://doi.org/10.1007/s40097-018-0291-4 (2019).
44. Tho, N. T. M. et al. Green synthesis of silver nanoparticles using *Nelumbo nucifera* seed extract and its antibacterial activity. *Acta Chim. Slov.* **60**, 673–678 (2013).
45. Fatimah, I. & Aftrid, Z. H. V. I. Characteristics and antibacterial activity of green synthesized silver nanoparticles using red spinach (*Amaranthus tricolor* L.) leaf extract. *Green. Chem. Lett. Rev.* **12**, 25–30. https://doi.org/10.1080/17518253.2019.1569729 (2019).
46. Gebru, H., Taddesse, A., Kausha, J. & Yadav, O. P. Green synthesis of silver nanoparticles and their antibacterial activity. *J. Surf. Sci. Technol.* **29**, 47–66 (2013).
47. Dayana, B. M. et al. Solution-gelation synthesis of silver nanoparticles utilizing *Justicia tranquebariensis* extract for antibacterial, antioxidant, antifungal and anticancer activity. *J. Sol-Gel Sci. Technol.* **110**, 828–841. https://doi.org/10.1007/s10971-024-06409-6 (2024).

48. Deivanathan, S. K. & Praksah, J. T. J. Synthesis of environmentally benign gold nanoparticles from *Vicoa indica* leaf extracts and their physiochemical characterization, antimicrobial, antioxidant and anticancer activity against A549 cell lines. *Res. Chem. Intermed.* **49**, 4955–4971. https://doi.org/10.1007/s11164-023-05114-3 (2023).
49. Alahmad, A. et al. *Hypericum perforatum* L.-mediated green synthesis of silver nanoparticles exhibiting antioxidant and anticancer activities. *Nanomaterials* **11**, 487. https://doi.org/10.3390/nano11020487 (2021).
50. Othman, A. M., Elsayed, M. A., Al-Balakocy, N. G., Hassan, M. M. & Elshafei, A. M. Biosynthesis and characterization of silver nanoparticles induced by fungal proteins and its application in different biological activities. *J. Genet. Eng. Biotechnol.* **17**, 8. https://doi.org/10.1186/s43141-019-0008-1 (2019).
51. Mohammed, A. E. et al. The antimicrobial activity of tea tree oil (*Melaleuca alternifolia*) and its metal nanoparticles in oral bacteria. *Peer J.* **12**, e17241. https://doi.org/10.7717/peerj.17241 (2024).
52. Forough, M. & Farhadi, K. Biological and green synthesis of silver nanoparticles. *Turk. J. Eng. Environ. Sci.* **34**, 281–287. https://doi.org/10.3906/muh-1005-30 (2010).
53. Manosalva, N. et al. Green synthesis of silver nanoparticles: effect of synthesis reaction parameters on antimicrobial activity. *World J. Microbiol. Biotechnol.* **35**, 88. https://doi.org/10.1007/s11274-019-2664-3 (2019).
54. Ulug, B., Turkdemir, M. H., Cicek, A. & Mete, A. Role of irradiation in the green synthesis of silver nanoparticles mediated by Fig (*Ficus carica*) leaf extract. *Spectrochim Acta Mol. Biomol. Spectrosc.* **25**, 135–161. https://doi.org/10.1016/j.saa.2014.06.142 (2014).
55. Donga, S. & Chanda, S. Facile green synthesis of silver nanoparticles using *Mangifera indica* seed aqueous extract and its antimicrobial, antioxidant and cytotoxic potential (3-in-1 system). *Artif. Cells Nanomed. Biotechnol.* **49**, 292–302. https://doi.org/10.1080/21691401.2021.1899193 (2021).
56. Jiang, C. H., Sun, T. L., Xiang, D. X., Wei, S. S. & Li, W. Q. Anticancer activity and mechanism of xathohumol: A prenylated flavonoid from hops (*Humulus lupulus* L). *Front. Pharmocol.* **9** https://doi.org/10.3389/fphar.2018.00530 (2018).
57. Wang, L. Y., Wu, M. Y., Wu, Z. Y. & Li, Y. T. Econazolium-gallate-econazole: the first econazole salt cocrystal registers dual optimizations in both physicochemical properties and antifungal efficacy. *J. Mol. Struct.* **1347**, 143355. https://doi.org/10.1016/j.molstruc.2025.143355 (2025).
58. Zhou, J. et al. Chrysotoxine regulates ferroptosis and the PI3K/AKT/mTOR pathway to prevent cervical cancer. 388 (2025) 119126. *J Ethnopharmacol* https://doi.org/10.1016/j.jep.2024.119126
59. Edison, T. N. J. I., Lee, Y. R. & Sethuraman, M. G. Green synthesis of silver nanoparticles using *Terminalia cuneata* and its catalytic action in reduction of direct yellow-12 dye. *Spectrochim Acta Mol. Biomol. Spectrosc.* **161**, 122–129. https://doi.org/10.1016/j.saa.2016.02.044 (2016).
60. Jain, A. S., Pawar, P. S., Sarkar, A., Junnuthula, V. & Dyawanapelly, S. Bionanofactories for green synthesis of silver nanoparticles: toward antimicrobial applications. *Int. J. Mol. Sci.* **22**, 11993. https://doi.org/10.3390/ijms222111993 (2021).
61. Ravichandran, V., Vasanthi, S., Shalini, S., Shah, S. A. A. & Harish, R. Green synthesis of silver nanoparticles using *Artocarpus altilis* leaf extract and the study of their antimicrobial and antioxidant activity. *Mater. Lett.* **180**, 264–267. https://doi.org/10.1016/j.matlet.2016.05.172 (2016).
62. Sarkar, S. & Kottesswaran, V. Green synthesis of silver nanoparticles from aqueous leaf extract of pomegranate (*Punica granatum*) and their anticancer activity on human cervical cancer cells. *Adv. Nat. Sci. Nanosci. Nanotechnol.* **9**, 025014. https://doi.org/10.1088/2043-6254/aac590 (2018).

Acknowledgements

The authors acknowledge St. Joseph's College Research Grant (SJCRG 2025-26) and DST-FIST, Government of India, for funding towards infrastructure and instrumentation facilities at ACIC, St. Joseph's College (Autonomous), Tiruchirappalli 620002. This work was supported by the National Research Foundation of Korea (NRF) grant funded by the Korean government (MSIT) (RS-2025-22222973).

Author contributions

B. Mary Dayana: Investigation, Writing - original draft. J. Thomas Joseph Prakash: Supervision, Writing—review and editing. Raja Venkatesan: Formal analysis, Methodology, Investigation, Writing—original draft. P. Saravanan: Methodology, Software. M. Sherlin Nivetha: Data curation, Writing—review and editing. Adhigan Murali: Investigation, Data curation, Writing—review and editing. Alexandre A. Vetcher: Investigation, Writing - original draft. Munusamy Settu: Resources, Software. Seong-Cheol Kim: Conceptualization, Supervision, Project administration, Funding acquisition, Writing—review and editing.

Declarations

Competing interests

The authors declare no competing interests.

Ethical approval

All experimental research and field investigations utilizing *Melaleuca alternifolia*, including plant material collection and exploitation, were carried out in strict accordance with applicable institutional, national, and international norms and legislation. This guarantees that the research follows the ethical and legal guidelines for using plants in scientific studies. The plant leaves *Melaleuca alternifolia* (Myrtaceae) was collected in January 2025 from the healthy plants in the hills of the Ooty district of Tamil Nadu, India. The herbarium was prepared by using plant material and Dr. M.R. Ganesh, Assistant Professor, Interdisciplinary Institute of Indian System of Medicine, SRM Institute of Science and Technology, Kattankulathur, Tamil Nadu 603203 India.

Consent for publication

All authors have indorsed the publication of this research.

Consent to participate

All person named as author in this manuscript have participated in the planning, design and performance of the research and in the interpretation of the result.

Additional information

Correspondence and requests for materials should be addressed to R.V., J.T.J.P. or S.-C.K.